Int. J. Electrochem. Sci., 10 **(2015)** 4832 - 4848

International Journal of
ELECTROCHEMICAL
SCIENCE
www.electrochemsci.org

Effect of Temperature on the Corrosion Behaviour of Super Austenitic Stainless Steel S32654 in Polluted Phosphoric Acid

Huabing Li[1,*], *Zhouhua Jiang*[1,**], *Hao Feng*[1], *Shucai Zhang*[1], *Peide Han*[2], *Wei Zhang*[3], *Guoping Li*[3], *Guangwei Fan*[3]

[1] School of Materials and Metallurgy, Northeastern University, Shenyang 110819, China
[2] College of Materials Science and Engineering, Taiyuan University of Technology, Taiyuan 030024, China
[3] Technology Center of Taiyuan Iron and Steel Croup Co. Ltd., Taiyuan 030001, China
[*]E-mail: lihb@smm.neu.edu.cn; jiangzh@smm.neu.edu.cn

Received: 7 March 2015 / *Accepted:* 28 March 2015 / *Published:* 28 April 2015

The effect of temperature on the corrosion behaviour of super austenitic stainless steel S32654 in polluted phosphoric acid was evaluated using open circuit potential monitoring, potentiodynamic polarization, potentiostatic polarization, electrochemical impedance spectroscopy and Mott-Schottky analysis. The open circuit potential, corrosion potential and passive current density all increase significantly, and the pitting potential decreases with increasing temperature. The induction period of pits is shortened with increasing temperature. Increasing temperature also promotes the dissolution of MnS inclusion and the metal matrix. EIS results reveal that the protection of passive film is predominantly attributed to the barrier film, and the passive film becomes more porous and less protective at higher temperatures. The passive film presents a bilayer structure and behaves as an n-type semiconductor and it becomes more defective at higher temperatures.

Keywords: Super austenitic stainless steel; Polluted phosphoric acid; Passive film; EIS; Mott-Schottky

1. INTRODUCTION

Phosphoric acid is a major chemical product, and 95% of phosphoric acid is manufactured by wet process phosphoric acid (WPA), including the main stages of the attack of phosphate ore by concentrated sulphuric acid (98 wt.%), filtration of the pulp and concentration of acid [1]. The process results in severe corrosion problems for the equipment due to the presence of impurities such as chlorides, fluorides, and sulfides [2-4]. So, the choice of materials with excellent corrosion resistance and mechanical properties is very important for the phosphoric acid industrial process. Considering the

trade-off of these properties, the austenitic stainless steel or nickel-based alloy with high alloying elements such as chromium, molybdenum, and nickel is a good choice for phosphoric media. 316L stainless steel is widely used for handling uncontaminated phosphoric acid at concentrations up to 85 wt.% and temperatures up to 93 ℃. The 317L and Alloy 20 are better choices than the 316L stainless steel. In more corrosive acids containing high concentrations of chloride, sulfate or fluoride, the high-alloyed super austenitic stainless steel 904L, 904hMo is developed. For severe service conditions such as in evaporators of a heat-exchanger operating at temperatures in excess of 90 ℃, the high-chromium-molybdenum austenitic stainless steels Alloy 28, Alloy 31 and nickel-based alloys Incoloy 825, Inconel 625 and Hastelloy G-30, G-35, C-276 are preferred selections in these severe service conditions [5,6]. Super austenitic stainless steel S31254 with 6 wt.% molybdenum was found to be substantially more resistant than Type 316L and 904L; it has relatively the same corrosion resistance as Hastelloy C-276 in phosphoric acid media in the absence and presence of chloride ions [7]. By further increasing the levels of chromium (24 wt.%), molybdenum (7.3 wt.%) and nitrogen content (0.5 wt.%), one of the most highly alloyed super austenitic stainless steels, S32654 (654SMO), has been developed. The PREN value, 57, of this steel is the highest among the super austenitic stainless steels. The steel with about double the strength of 316L stainless steel exhibits excellent corrosion resistance in inorganic and organic acids or acids containing chloride, with a similar or preferable levels to many of the nickel-based alloys [8-12]. In these cases, S32654 is an alternative to other considerably more expensive nickel-based alloys in WPA.

The excellent corrosion resistance of austenitic stainless steel is attributed to the formation of thin and compact passive films, which prevent the metals from reacting with aggressive environments. It is well known that stainless steels have a stable passive film with rapid passivation ability even in severe corrosive conditions. Alloying elements such as Cr, Mo, Ni and N play an important role in the composition and structure of protective passive films [13,14]. Cr is the key element in enforcing passivity, and its enforced passivity appears to be due to its rich inner oxide layer (the barrier layer). Ni could decrease the overall dissolution rates of Fe and Cr [15]. Mo exhibits a strong beneficial role on the corrosion resistance of stainless steels due to the presence of MoO_3 in the outer layer of the passive film and the formation of insoluble oxides [16]. Nitrogen is the strongest beneficial element on local corrosion. The presence of nitrogen in the form of nitrites, nitrides, NH_3 or NH_4^+ in the passive films greatly decreases the dissolution of metals [17-19]. Additionally, the synergistic effects of nitrogen and molybdenum further buffer the pH and stabilize the molybdates; the molybdates assist in the formation of NH_3 and NH_4^+ [20-22]. Much research has been completed on the properties of passive films formed on austenitic stainless steels with different alloying elements in an aqueous acid solution [23-25].

In recent years, several references on the corrosion behaviour and semiconducting properties of passive films for austenitic steel in phosphoric acid contaminated with sulphate, chloride or fluoride ions have been published [26-31]. Escrivà-Cerdán [26,29] revealed that the stability of the passive film decreased with increasing temperature in phosphoric acid polluted with sulphate, chloride, and fluoride ions. The stability decrease is attributed to the fluoride ions that were incorporated into the passive film formed on Alloy 31 and its concentration as temperature increased, resulting in the reduction of chromium species. Higher temperature tends to promote the formation of a porous polyphosphate film,

which results in an increase of the thickness but a decrease of the corrosion resistance. However, there is scarcely any information available on the corrosion behaviour and electrical properties of S32654 in polluted phosphoric acid.

The main aim of the present research is to evaluate the corrosion behaviour of a newly developed super austenitic stainless steel, S32654, in phosphoric acid polluted with sulphate and chloride ions. The electrochemical behaviour, passivation kinetics, and semiconducting properties were examined at different temperatures (20, 40, 60, and 80℃) to reveal the effect of temperature on the corrosion behaviour of the steel in simulated typical industrial conditions.

2. EXPERIMENTAL

2.1 Material and test solution

The material tested was a newly developed super austenitic stainless steel S32654 provided by Taiyuan Iron and Steel Croup Co. Ltd. with higher molybdenum and nitrogen contents. The steel was manufactured using a vacuum induction-melting furnace, followed by an electroslag-remelting furnace to obtain low sulfur content. The electroslag remelting ingot was kept at 1280 ℃ for 10 h, and then the sample was hot forged and hot rolled into a 6 mm thick plate. The chemical composition of the steel is shown in Table 1.

Table 1. Chemical composition of the super austenitic stainless steel S32654 (wt%)

Steel	C	Cr	Ni	Mo	Cu	Mn	N	Si	P	S
S32654	0.015	23.36	21.75	7.46	0.46	3.40	0.42	0.22	0.007	0.001

The specimens of 10.1 mm×10.1 mm were machined from the hot rolled plate and then were solution annealed at 1200 ℃ for 1 h followed by water quenching. The passivation treatment of the specimens was performed in 20-30 wt.% nitric acid solution at 50 ℃ for 1 h to prevent the occurrence of crevice corrosion at high temperature. The electrodes were mounted in epoxy resin with an exposed area of 1 cm^2 and polished with SiC paper from 200 to 2000 grits.

All of the electrochemical tests were performed in polluted 40 wt.% phosphoric acid solution with 2 wt.% H_2SO_4 and 0.06 wt.% KCl, which is typical in the phosphoric acid industry[27,28].

2.2 Experimental methods

The solution annealed S32654 was etched using 10 wt.% oxalic acid and then examined by a Carl Zeiss Axio Imager M1m optical microscope (OM) to obtain its microstructure. The typical inclusions were analysed by a Carl Zeiss Ultra Plus Field Emission scanning electron microscope (SEM) and an energy dispersive spectrometer (EDS).

All of the electrochemical measurements were carried out using a Gamry Reference 600 potentiostat, which was comprised of three electrodes. The S32654 stainless steel specimen was the working electrode, and a platinum foil (Pt) and a saturated calomel electrode (SCE) were used as the counter and reference electrodes, respectively. All electrochemical measurements were performed at 20, 40, 60, and 80 ℃ to investigate the effect of temperature on the corrosion behaviour of S32654 in the polluted phosphoric acid environment. The experiment temperature was accurately controlled using a HH-601 super thermostatic water bath.

The open circuit potential was measured for 2 h in the test solution. The average value of the potentials obtained during the last 300 s was regarded as the value of the OCP, according to ASTM G-5 [32]. The potentiodynamic polarization curves of S32654 were completed under different temperatures from -0.2 V below the OCP with a scan rate of 20 mV min^{-1} to the anodic direction. Potentiostatic polarization measurements were performed to obtain the relationship between the current transient and the time at a constant applied potential. Prior to each measurement, the working electrode was initially kept potentiostatically at -1.0 V_{SCE} for 600 s to remove the passive film formed in the air. Then, the chosen potential (0.6 V_{SCE}) was applied for 15000 s and the potentiostatic current density transients were recorded.

The working electrode was passivated under the potential of 0.6 V_{SCE} for the electrochemical impedance spectroscopy (EIS) and capacitance measurements. EIS measurements were carried out in the frequency range between 100 kHz and 0.01 Hz with voltage amplitude of 10 mV. The impedance spectra were fitted with ZSimpWin software. The capacitance measurements of the passive films formed at 0.6 V_{SCE} were completed with amplitude voltage of 5 mV in the potential ranges from 0.6 to -0.2 V_{SCE} by 40 mV steps in the cathodic direction.

3. RESULTS & DISCUSSION

3.1 Microstructure examination

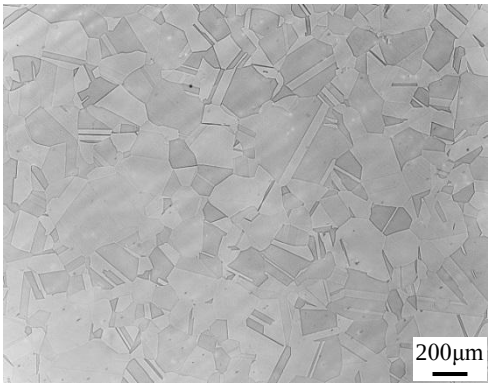

Figure 1. Optical microscopy of solution annealed S32654

Fig. 1 shows the microstructure of the solution annealed S32654 super austenitic stainless steel. The equiaxed grains with annealing twins can be obviously observed, which reveals that the

microstructure of the solution annealed steel consists of a single austenitic phase. However, the sulphur (0.0015 wt.%) and manganese (3.4 wt.%) content of S32654 is lower. The typical non-metallic MnS inclusions with a size of less than 2 μm and the MnS inclusions around the Al_2O_3 inclusions can be determined by the BSE images and the EDS analysis, as shown in Fig. 2.

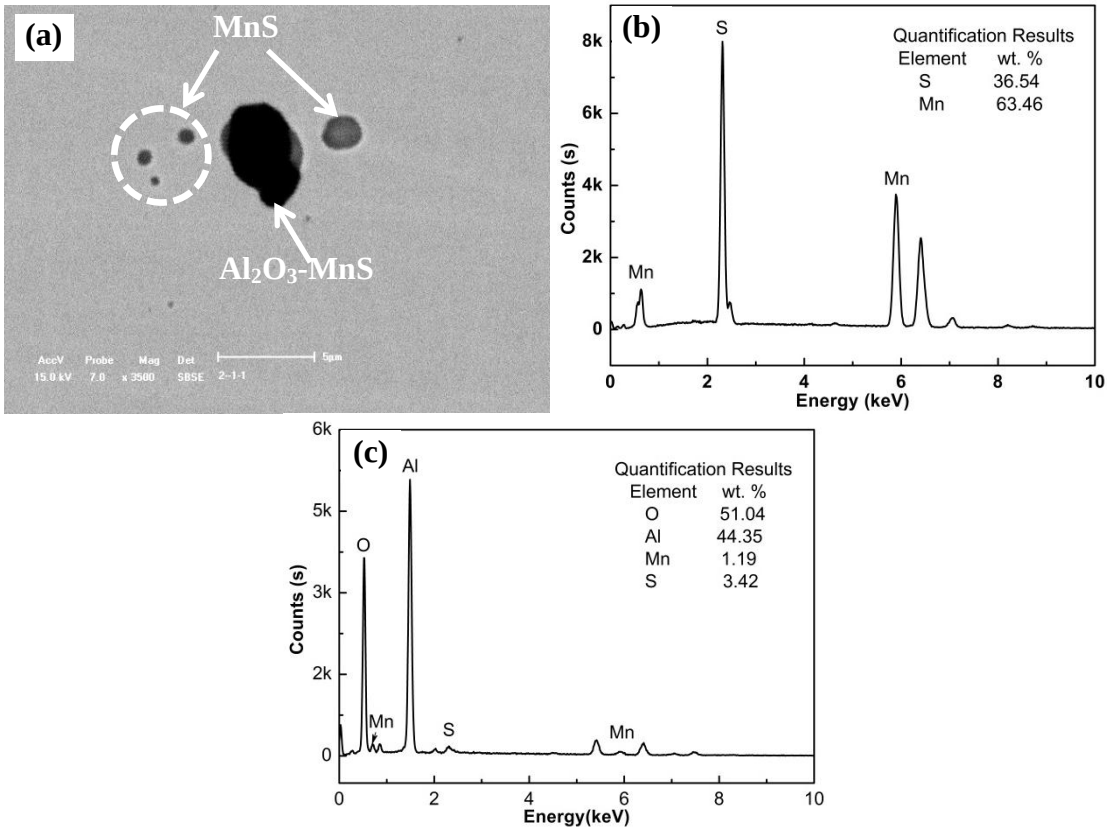

Figure 2. (a) BSE (backscattered electron) images of typical inclusions and (b) EDS analysis for MnS inclusion and (c) Al_2O_3-MnS

3.2 Open circuit potential results

Fig. 3 shows the open circuit potential measurement for S32654 in polluted phosphoric acid solution investigated at 20, 40, 60 and 80 ℃. The potential shifting towards more positive values with prolonged time at all temperatures is attributed to the healing of oxide film formed in the pre-immersion air and further thickening of that film as a result of the interaction between the electrolyte and the metal surface [26,33]. The growth of oxide film continues until the film obtains a thickness that is stable in the electrolyte. Furthermore, the potential with time exhibits a steady increase at temperatures ranging from 20 to 60 ℃, which indicates that the passive films formed on the S32654 at temperatures lower than 60 ℃ have good corrosion resistance during the immersion in the polluted phosphoric acid solution. The fluctuated potential values with occasional rise and fall in the active region at 80 ℃ can be related to nucleation and repassivation of the pits and/or crevices on the surface of the S32654 [34,35]. Table 2 summarizes the steady OCP values of S32654 in the polluted

phosphoric acid solution at different temperatures. It can be seen that OCP values shift toward more positive potential values with increasing temperature. It is a well-known fact that higher temperature accelerates the kinetics of corrosion reactions, but it also promotes the rapid growth of passive films on metallic surfaces. The passive films then become thicker [34,36], which causes the ennoblement of the metal.

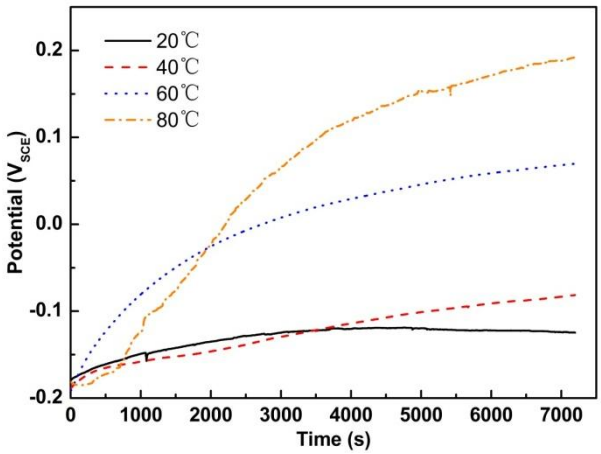

Figure 3. Evolution of the open circuit potential with time for S32654 in polluted phosphoric acid

Table 2. Open circuit potential values for S32654 in polluted phosphoric acid

Temperature(℃)	E_{st} (mV_{SCE})
20	-124.2
40	-82.9
60	68.5
80	189.5

S32654 contains 23.36 wt.% chromium, which is favourable for metal passivation. Higher content molybdenum with 7.46 wt.% could more easily form solid molybdate compounds in the outer regions of the passive film. This molybdate layer is cation selective, and it resists the incorporation of aggressive anions such as Cl^-, allowing for the growth of a chromium oxide inner barrier layer [34]. Additionally, the high nitrogen content with 0.42 wt.% in the steel can further promote molybdenum enrichment in the passive films, which improves the stability and compactness of the passive films [37]. Thus, the OCP value shifted towards more positive values during the OCP measurements.

3.3 Potentiodynamic polarization results

Fig. 4 represents that the potentiodynamic polarization curves in polluted phosphoric acid in the temperature range from 20 to 80 ℃. There are obvious passivation ranges at all temperatures, indicating that S32654 exhibits excellent corrosion resistance in the polluted phosphoric acid solution

[27]. Thus, the potential 0.6 V_{SCE} was chosen in the passivation range to investigate the properties of passive films formed on S32654. On the anodic branch of the curve, the absence of active current peak and Flade potential confirms the passive films previously formed on S32654 in the air maintain their passivity in the polluted phosphoric acid solution [38]. The current density rapidly increases, and the pitting corrosion occurs when increasing the potential to a critical value of 1.0 V_{SCE}.

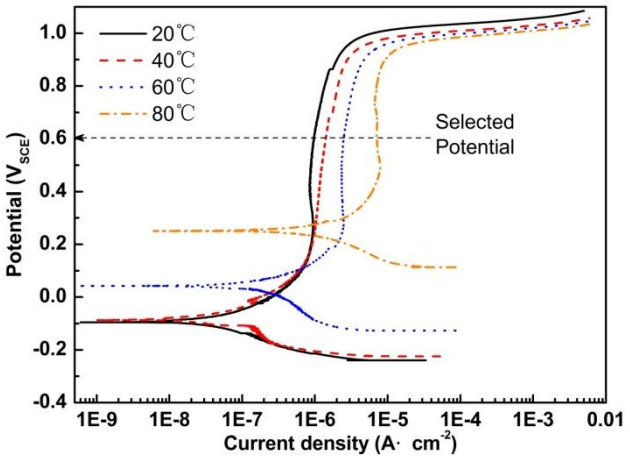

Figure 4. Potentiodynamic polarization curves for S32654 in polluted phosphoric acid

The temperature dependence of the cathodic reaction can be observed due to the cathodic current densities increasing with temperature; furthermore, the cathodic current densities exhibit an obvious increment in the temperature range from 40 to 80 ℃. The phenomenon demonstrates that increasing temperature favours the cathodic reaction as well as the hydrogen evolution reaction (HER) [36]. The kinetics of anodic dissolution of the steel is also favoured with increasing temperature, owing to the increase of the anodic current densities at higher temperature. Although, higher current densities in the passivation range promote the growth of passive films formed on S32654.

From the potentiodynamic curves, the values of corrosion potential (E_{corr}), corrosion current density (i_{corr}), the values of tafel slopes (β_a, β_c), passive current density (i_p) and pitting potential ($E_{b,100}$) were obtained and listed in Table 3. With increasing of the temperature, the values of E_{corr}, i_{corr}, β_a and i_p were shifted to higher values. And the values of β_c presented increasing trend. The increasing of E_{corr} with temperature is related to the increment of the cathodic current density [36], and the tendency of E_{corr} is consistent with that of OCP. The values of i_{corr} exhibit a slight increase in the temperature range from 20 to 40 ℃ and an abrupt increase from 40 to 80 ℃, which indicates that aggressive ions accelerate the corrosion of metals at elevated temperatures.

The increment of i_p values with temperature affirms that higher temperature promotes the kinetics of the passivation reaction, which is favourable for the growth of passive films [26,27]. The $E_{b,100}$ is defined as the potential at which the current density arrives at 100 μA/cm^2; it significantly decreases with increasing temperature. So, S32654 exhibits decreasing corrosion resistance as temperature increases in the polluted phosphoric acid solution. The results represent that the anodic dissolution of this steel is accelerated, and the protective properties of the passive film formed on

S32654 become more defective at higher temperatures. The main composition changes of the passive films with increasing temperature are responsible for the decrement in the protective properties of the films formed at higher temperatures [39]. The porosity increment is another of the main changes in the passive film properties with increasing temperature, porosity being a potential factor leading to poorer film protectiveness. The temperature increment causes the passive film to become thinner and more porous and less protective. The lower $E_{b,100}$, the higher i_p and the narrower passivation ranges with increasing temperature reflect this fact. Several authors have reported similar results [27, 40-43].

Table 3. Potentiodynamic polarization parameters for S32654 in polluted phosphoric acid

Temperature(℃)	E_{corr} (mV_{SCE})	i_{corr} ($\mu A \cdot cm^{-2}$)	β_a(V)	β_c(V)	i_p ($\mu A \cdot cm^{-2}$)	$E_{b,100}$ (mV_{SCE})
20	-93.32	0.061	0.107	0.124	0.96	1035.4
40	-52.32	0.072	0.121	0.186	1.40	1009.0
60	43.57	0.216	0.133	0.195	2.49	998.0
80	246.86	1.341	0.183	0.157	7.04	985.0

3.4 Potentiostatic polarization results

The current-time transients of S32654 obtained in polluted phosphoric acid solution at different temperatures are shown in Fig. 5. The values of current transient density give the total current resulting from the formation and dissolution of the passive film on S32654 in the present solution [44]. It can be observed that the current density initially decreases rapidly with time at all temperatures. This is attributed to the nucleation and growth of the passive films formed on S32654 at a rate higher than that of dissolution [45-47]. All of the current-time transients show further increment of time result in a relatively steady state current density (i_{ss}), indicating the formation of passive films on the surface of S32654 at all temperatures. At 20 and 40 ℃, the current densities show a steady decrement tendency, which can be attributed to the formation of intact passive films that provide very good protection for S32654. However, the significant current density fluctuations of the current-time transients can be observed at 60 and 80 ℃, which is related to either nucleation or metastable pitting events [48,49]. The i_{ss} is observed to increase with temperature, indicating the decrease of the protective ability of the passive film. In addition, increasing temperature results in shortening the time of current density fluctuation; this means that the induction period of the pits is shortened, and the corrosion process is accelerated at higher temperatures.

Fig. 6 shows the microscopic morphology for S32654 after potentiostatic polarization in polluted phosphoric acid at different temperatures. With increasing temperature, the pits can be clearly seen, and the amount and size of pits increase. These changes are attributed to the presence of aggressive ions such as chloride, sulphate in solution, and the acceleration of the dissolution of metal at higher temperatures [26,50].

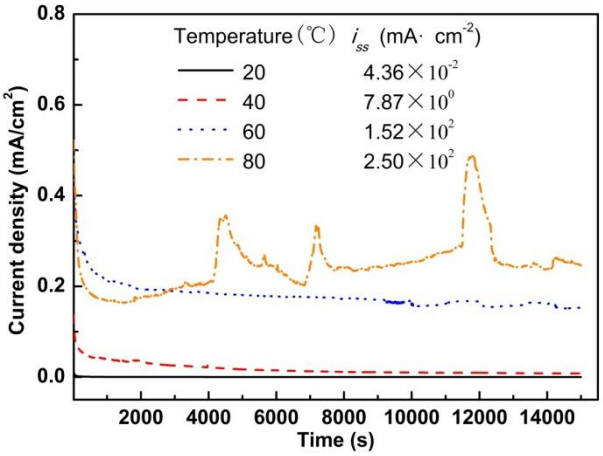

Figure 5. Potentiostatic polarization curves for S32654 in polluted phosphoric acid

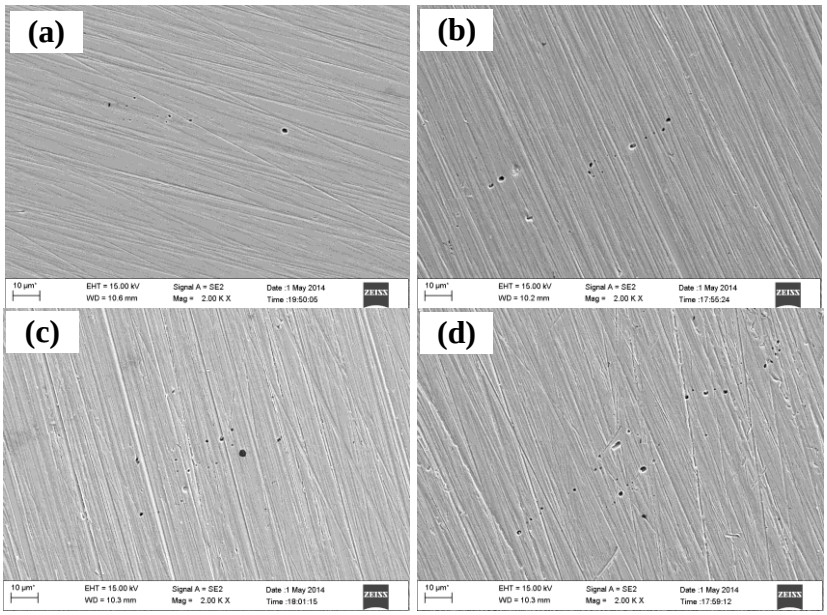

Figure 6. Microscopic morphology for S32654 after potentiostatic polarization in polluted phosphoric acid (a) 20 ℃; (b) 40 ℃; (c) 60 ℃; (d) 80 ℃.

The typical corrosion pit morphology was observed using SEM after potentiostatic polarization, as shown in Fig. 7(a). There typically exit two types of pits for a single morphology; another pit type occurs around the Al_2O_3-MnS composite inclusions analysed by the EDS, as shown in Fig. 7(b). For stainless steel, the location of the corrosion pits is associated with the inclusions and second phase precipitates [51-53]. Compared with other non-metallic inclusions, the MnS inclusion acting as pit predominantly preferential nucleation site is the most detrimental to corrosion resistance. These results indicate that the preferential adsorption of aggressive ions, such as chloride ions, onto the MnS inclusion results in the dissolution of the inclusions and the metal [54]. Noh et al. [55] suggested that MnS inclusions are preferred sites for pit initiation, especially when the sites are physically associated with another type of inclusion, such as oxide or silicate. From Fig. 7(a), pits with sizes less

than 2 μm can be attributed to the dissolution of the pure MnS inclusions; pits around the Al_2O_3 inclusion with a small amount of residual MnS ascribe to the preferential partial dissolution of MnS. The dependence of pits on temperature can be interpreted that by increasing the temperature in the polluted phosphoric acid; the dissolution of the MnS inclusion and the metal matrix are promoted, and the amount of pits increase and become larger, as observed in Fig. 6.

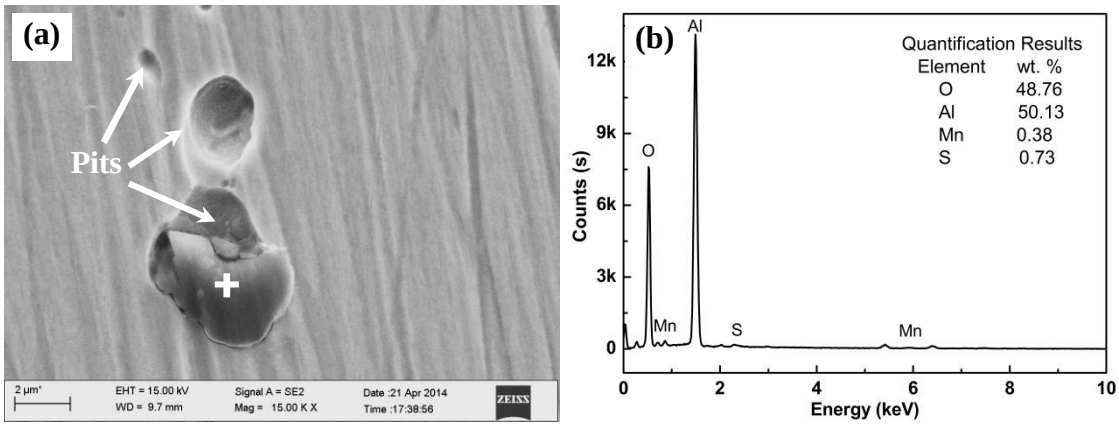

Figure 7. Typical corrosion morphology (a) and EDS analysis (b) for inclusion

3.5 EIS results

For a better understanding of the effect of temperature on the stability of the passive films formed on S32654 in polluted phosphoric acid, EIS tests were performed after passive films generation at 0.6 V_{SCE} for 1 h at different temperatures. Nyquist and Bode plots are presented in Fig. 8. All Nyquist plots exhibit a depressed semicircle, which is attributed to the distribution of the relaxation times resulting from surface heterogeneities, species adsorption, and porous layer formation [56-58]. With increasing temperature, the decrease in the diameter of depressed semicircle is obvious, indicating the decrease of the protective properties of passive films.

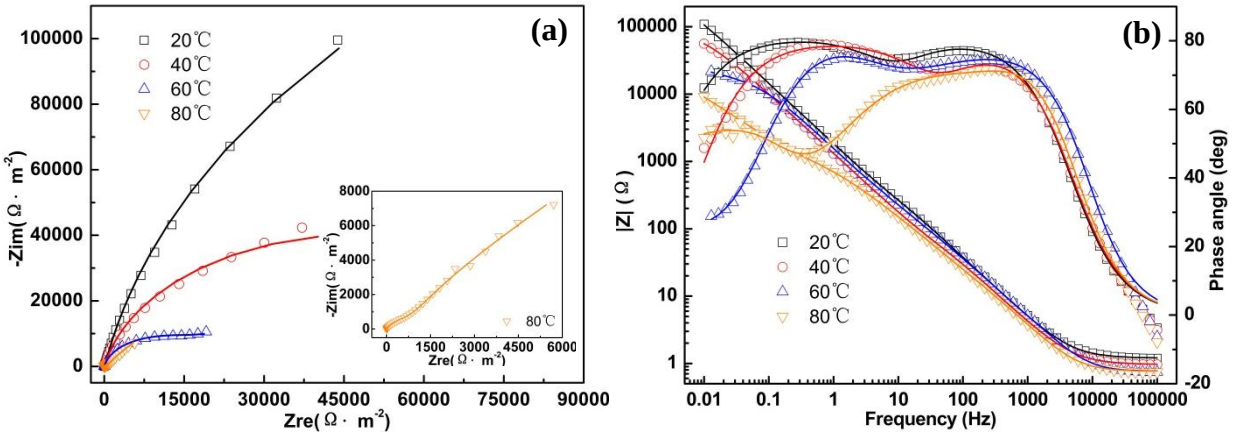

Figure 8. EIS for S32654 in polluted phosphoric acid: (a) Nyquist plots; (b) Bode plots

From the inserted graph in Fig. 8(a), the Nyquist plot at 80℃ shows a typical semicircle with a 45° straight line. The line represents the Warburg impedance, and the corrosion process is controlled by a diffusion process [59,60].

From Fig. 8 (b), a decrease in the impedance modulus values are seen at the low frequency region representing the electrode polarization resistance and revealing that the stability of the passive film deteriorates; the corrosion rate increases with the impedance modulus decrease. The modulus values are all lower than 90°, indicating a deviation from ideal capacitor behaviour. The constant phase element (CPE) is necessary to account for the non-ideal behaviour of the capacitive elements. Bode plots at temperatures from 20 to 60 ℃ exhibit two phase angles corresponding to two time constants. Therefore, the passive films formed on S32654 have a bilayer structure [38]. However, there exists three phase angles at 80 ℃, and the third time constant is related to the diffusion processes through the passive films.

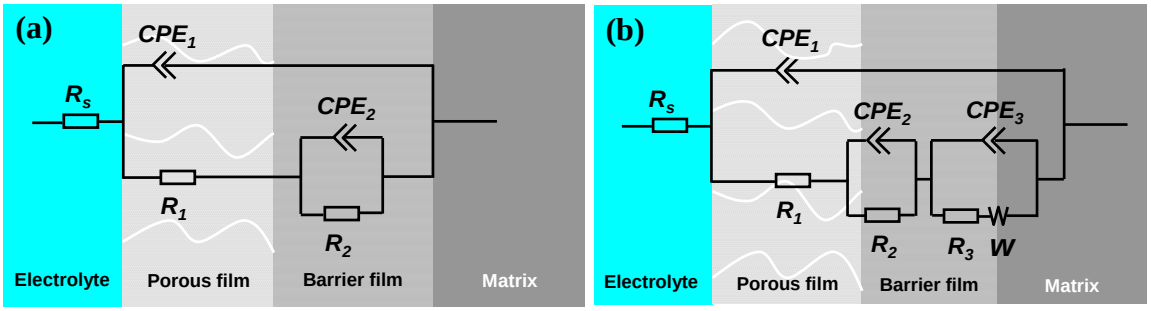

Figure 9. Equivalent circuits for the interpretation of EIS spectra obtained at different temperature (a) from 20 to 60 ℃; (b) 80 ℃

Table 4. Equivalent circuit parameters for S32654 in contaminated H_3PO_4

Temperature (℃)	R_{sol} (Ω cm^2)	Q_1 Y_0 10^{-5} (S s^n cm^{-2})	n_1	R_1 (Ω cm^2)	Q_2 Y_0 10^{-5} (S s^n cm^{-2})	n_2	R_2 (kΩ cm^2)	Q_3 Y_0 10^{-4} (S s^n cm^{-2})	n_3	R_3 (Ω cm^2)	W Y_0 10^{-4} (S s$^{0.5}$ cm^{-2})
20	1.196	8.051	0.900	1274	2.440	0.907	393.2	-	-	-	-
40	0.964	9.801	0.897	184.9	5.024	0.874	95.75	-	-	-	-
60	0.752	6.454	0.921	128.7	6.988	0.770	26.47	-	-	-	-
80	0.760	7.310	0.938	29.55	22.41	0.665	1.247	7.268	0.996	1588	3.526

From the Nyquist plots (Fig. 8(a)) and the Bode plots (Fig. 8(b)), it is obviously distinguishable that two types of equivalent circuits are necessary for the analysis of impedance spectra data. The equivalent circuit $R_s(CPE_1(R_1(CPE_2R_2)))$ and $R_s(CPE_1R_1(CPE_2R_2)(CPE_3(R_3W)))$ were chosen to fit the EIS data obtained for the temperatures ranging from 20 to 60 ℃ and 80 ℃, as shown in Fig. 9. The results of the fitting parameters are listed in Table 4. The fitting curves are plots as solid lines in the Nyquist and Bode plots, as shown Fig. 8, which are in good agreement with the experimental results.

In the circuits, R_s represents the electrolyte resistance and CPE_1 and R_1 are the capacitance and resistance of the outer porous film, respectively. CPE_2 and R_2 are the capacitance of the inner compact passive film (barrier film), respectively, and R_3 corresponds to the charge transfer resistance. CPE_3 is associated with the capacitance of the inner compact passive film/matrix interface, and W is the diffusion impedance through the passive film layer.

According the fitting parameters shown in Table 4, the R_2 value of the inner compact passive film (barrier film) is much larger than the R_1 value of the outer porous film. This indicates that the passive film protection is predominantly attributed to the barrier film, which is consistent with other reports on stainless steels [30,31]. The R_1 and R_2 values obviously decrease with an increased solution temperature, primarily, and there exists an abrupt decrease in these values at 80 ℃. The decrease of polarization resistance and increase of Q_2 indicate that the temperature increase results in the thinning of the passive films, and being more porous and having a less protective film structure. Thus, the absorption of the intermediate species through the passive film becomes easier at higher temperatures (80 ℃).

In highly concentrated H_3PO_4 media, phosphates species can precipitate with dissolved iron species to form iron phosphates because the solubility of these compounds is low. Precipitation of iron phosphate occurs at the interface[61], according to the following equation:

$$6H_3PO_4 + 3Fe \rightarrow 3Fe(H_2PO_4)_2 + 3H_2 \quad (1)$$

$$3Fe(H_2PO_4)_2 \rightarrow Fe_3(PO_4)_2 + 4H_3PO_4 \quad (2)$$

For stainless steels, due to the low oxidative capacity of the surface in phosphoric acid solutions[62], a predominant formation of a phosphate compound $Fe(H_2PO_4)_2$ occurs. This compound is mainly responsible for the outer porous film formation.

S32654 has a high chromium and nickel content, as other research has been reported [30,31,34]. Chromium oxide (Cr_2O_3) and nickel oxide (NiO) should form in the inner passive film, which is compact and accountable for the corrosion resistance. Moreover, the higher molybdenum content leads to the formation of insoluble MoO_3 in the outer passive film in a strong acidic solution [16]. Concurrently, the presence of Mo raises the Cr content in the inner oxide layer [34]. Many studies have reported that in nitrogen-containing austenitic stainless steels, the nitrogen enriches on the surface of the passive film in the form of NH_3 or NH_4^+, which effectively buffer the local pH, promote the repassivation, and depress oxidation inside a pit [17-19]. Other authors have also reported the presence of nitrides such as CrN or Cr_2N in the passive film of nitrogen alloying stainless steels due to the anodic segregation [17,21]. The occurrence of the following reaction is possible and results in the formation of NH_3 ligands, or perhaps NH_4^+ *via* further protonation. The reaction also lowers the pH in the pits and mitigates the environment. In the present work using S32654 with 0.42 wt.% nitrogen content, the NH_3, NH_4^+, CrN or Cr_2N should exist in the outer passive film. The structure and composition of the passive film of S32654 will be examined in the future research.

$$2CrN + 3H_2O \rightarrow Cr_2O_3 + 2NH_{3,ligand} \quad (3)$$

3.6 Mott-Schttky analysis

It is well recognized that there is a relationship between the semiconducting properties and the corrosion resistance of passive films [63,64]. According to much literature, the passive films formed on stainless steels exhibit semiconducting properties [65-68], which can be well described by the Mott-Schottky (M-S) analysis. To investigate the temperature effect on the electronic properties of the passive film formed on S32654 in the polluted phosphoric acid solution, the M-S analysis was performed after the specimens were passivated at 0.6 V_{SCE} for 1 h.

Based on the Mott-Schottky theory [65], the semiconducting properties can be determined by analysing the capacitance as a function of the applied potential, which reflects the charge distribution in the passive films. The Mott-Schottky relationships for n-type and p-type semiconductors are expressed below by Eqs. (4) and (5), respectively.

$$\frac{1}{C^2} = -\frac{2}{\varepsilon\varepsilon_0 q N_A}\left(E - E_{FB} - \frac{kT}{q}\right) \quad \text{（p type）} \qquad (4)$$

$$\frac{1}{C^2} = \frac{2}{\varepsilon\varepsilon_0 q N_D}\left(E - E_{FB} - \frac{kT}{q}\right) \quad \text{（n type）} \qquad (5)$$

where C is the space charge capacitance, ε is the dielectric constant of the passive film(15.6), ε_0 is the permittivity of free space (8.854×10^{-14} F/cm), q is the electron charge(1.602×10^{-19} C), N_D and N_A are the donor and acceptor densities, respectively. E_{FB} is the flat band potential, k is the Boltzmann constant (1.38×10^{-23} J/K), and T is the absolute temperature. N_D and N_A can be determined from the slope of the experimental $1/C^2$ vs. the applied potential (E).

Fig.10 shows the M-S curves for the passive films formed on S32654 in polluted phosphoric acid at 20, 40, 60, and 80℃. Firstly, it is all clearly noted that capacitance increases with the solution temperature, which is consistent with the results of the potentiostatic polarization curves and EIS measurements. In the potential range of 0.25 to 0.45 V_{SCE}, there exists a linear relationship that can be found between C^{-2} and E at all temperatures. Within this potentials range, the positive slopes suggest that the passive film formed on S32654 behaves as an n-type semiconductor, which can be attributed to the outer porous iron-rich layer or the presence of other compounds due to the effect of phosphates [30,31].

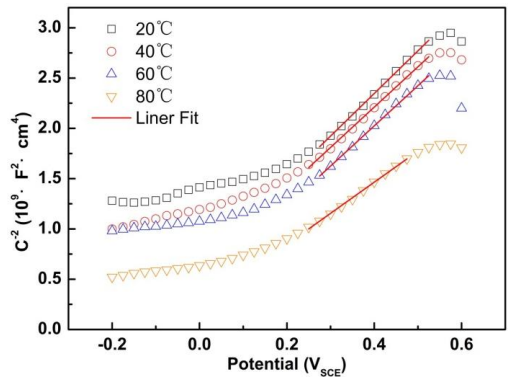

Figure 10. Mott-Schottky plots for S32654 in polluted phosphoric acid

According to Eq. (5), the donor density N_D can be determined from the slope of C^{-2} vs. E plots and the E_{FB} from the extrapolation of liner potion to C^{-2} =0. The obtained values are listed in Table 6. The donor density values are on the order of 10^{21} cm^{-3}, which agree well with the values obtained by other researchers [26,65]. N_D increases with temperature can be observed exhibiting that higher donor densities lead to higher current density values in the passive region at elevated temperatures. The results are consistent with the polarization curves and the current-time transients. According to the Point Defect Model (PDM) [69,70], the donors or acceptors in the semiconducting passive films are the defects themselves, including cation vacancies, anion vacancies, and metal interstitials. Cation vacancies are electron acceptors thereby doping the barrier layer p-type; however, anion vacancies (oxygen vacancies) and metal interstitials are electron donors, resulting in n-type doping. The presence of such dopants prevents the migration of cations from the metal substrate and the penetration of harmful anions, such as Cl^- and SO_4^{2-}, from the electrolyte, thereby improving the corrosion resistance. With increasing solution temperature, the kinetics of the passivation reaction is accelerated, and the oxygen vacancies concentration increases as the dominant donor species increase. Thus, high donor densities indicate the highly disordered nature of passive films and low impedance [28]; both of the outer layers of passive films formed on S32654 become more defective with increasing solution temperature, as observed in the EIS measurements. Moreover, the E_{FB} decreases when the temperature increases.

Table 4 Donor density and flat band potential values for S32654 in polluted phosphoric acid

Temperature(℃)	*Slope*	N_D (cm^{-3})	E_{FB} (V_{SCE})
20	4.05×10^{9}	2.236×10^{21}	-0.181
40	3.93×10^{9}	2.303×10^{21}	-0.163
60	3.76×10^{9}	2.407×10^{21}	-0.140
80	2.98×10^{9}	3.039×10^{21}	-0.090

Furthermore, the thickness of the space charge layer (W) of an n-type semiconductor at a film formation potential can be calculated by the following equation [25,71].

$$W = \left[\frac{2\varepsilon\varepsilon_0}{eN_D}(E - E_{FB} - \frac{kT}{e})\right]^{1/2} \quad (6)$$

Fig. 11 shows the relationship between the space charge layer thickness and the applied potential E for passive films formed on S32654 at 0.6 V_{SCE} for 1 h in polluted phosphoric acid. The thickness of the space charge layer decreases with increasing temperature. The previous research suggests that the space charge layer is an effective barrier to the flow of carriers, such as electrons and vacancies from semiconductor to electrolyte, and the pitting corrosion resistance of steel is improved with an increased thickness of the space charge layer [71,72]. Thus, it can be concluded that the decrease of the space charge layer thickness of passive films formed on S32654 indicates that the passive films exhibit poor protective ability for corrosion resistance at elevated temperatures.

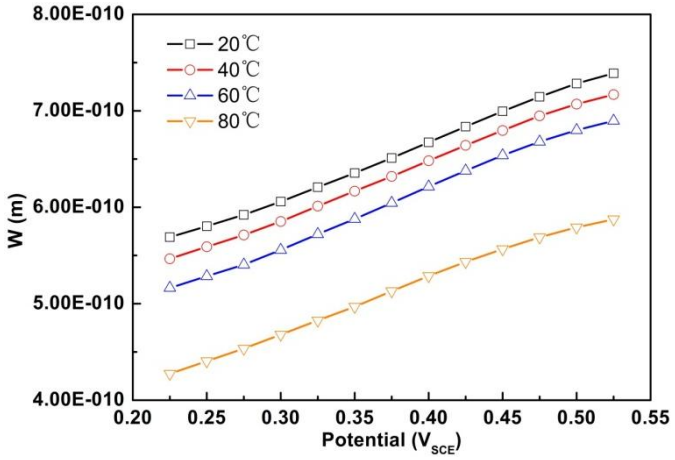

Figure 11. Relation between the space charge layer thickness and the applied potential

4. CONCLUSION

The effect of temperature on the corrosion behaviour of super austenitic stainless steel S32654 in polluted phosphoric acid was investigated. The main conclusions are summarized as follows:

(1) S32654 exhibits passivation ranges at all temperatures. The open circuit potential, corrosion potential, and passive current density each increase significantly, and the pitting potential decreases with increasing temperature. The results indicate that the corrosion process is accelerated at higher temperatures.

(2) The steady state current densities increase, and the induction period of the pits is shortened with increasing temperature. These results indicate that the protective ability of the passive film decreases, and the corrosion process is accelerated. Increasing temperature of the polluted phosphoric acid solution promotes the dissolution of MnS inclusion and the metal matrix; the number of pits increases, and the pit sizes become larger.

(3) The EIS results reveal that the protection of the passive film is predominantly attributed to the barrier film. The polarization resistance of the passive film obviously decreases with increasing temperature, indicating the passive film becomes more porous and less protective at higher temperatures.

(4) The Mott-Schottky analysis shows that the passive film formed on S32654 in polluted phosphoric acid presents a bilayer structure and behaves as an n-type semiconductor. The donor densities increase and the space charge layer thickness decreases with temperature. Therefore, the passive films become more defective, resulting in decreased protective abilities of the passive films.

ACKNOWLEDGEMENTS

The present research was financially supported by National Key Technology Research and Development Program of the Ministry of Science and Technology of China (No. 2012BAE04B01), High Technology Research and Development Program of China (No. 2015AA034301), National Natural Science Foundation of China(No.51304041), China Postdoctoral Science Foundation(No. 2013M530936) and Program for New Century Excellent Talents in University(No. N130502001).

Reference

1. P. Becker, Phosphates and phosphoric acid. raw materials, technology, and economics of the wet process, 2nd Edn., CRC Press, New York 1989
2. A. Bellaouchou, A. Guenbour, A. Benbachir, *Corrosion*, 49 (1993) 656
3. S. El Hajjaji, L. Aries, J. P. Audouard, F. Dabosi, *Corros. Sci.*, 37 (1995) 927
4. H. Iken, R. Basseguy, A. Guenbour, A. Ben Bachir, *Electrochim. Acta*, 52 (2007) 2580
5. C. M. Schillmoller, Alloy selection in wet process phosphoric acid plants, NiDl technical series No.10015
6. A. C. Hart, *Br. Corros. J.*, 6 (1971) 205
7. L. de Micheli, A. H. P. Andrade, C. A. Barbosa, S. M. L. Agostinho, *Br. Corros. J.*, 34 (1999) 67
8. J. Olsson, W. Wasielewska, *Mater. Corros.*, 48 (1997) 791
9. B. Wállen, M. Liljas, P. Stenvall, *Mater. Des.*, 13 (1992) 329
10. B. Wallén, M. Liljas, P. Stenvall, *Mater. Corros.*, 44 (1993) 83
11. E. Aragona, J. Woillez, C. Perice, F. Tabaries, M. Sitz, *Mater. Des.*, 30 (2009) 1548
12. http://www.valve-world.net/pdf/11021.pdf
13. Y. S. Zhang, X. M. Zhu, S. H. Zhong, *Corros. Sci.*, 46 (2004) 853
14. C. O. A. Olsson, D. Landolt, *Electrochim. Acta*, 48 (2003) 1093
15. V. Maurice, W. P. Yang, P. Marcus, *J. Electrochem. Soc.*, 145 (1998) 909
16. A. Pardo, M. C. Merino, A. E. Coy, F. Viejo, R. Arrabal, E. Matykina, *Corros. Sci.*, 50 (2008) 780
17. I. Olefjord, L. Wegrelius, *Corros. Sci.*, 38 (1996) 1203
18. S. D. Chyou, H. C. Shih, *Mater. Sci. Eng. A*, 184 (1991) 241
19. H. J. Grabke, *ISIJ Int.*, 36 (1996) 777
20. C. O. A. Olsson, *Corros. Sci.*, 37 (1993) 467
21. Y. C. Lu, M. B. Ives, C. R. Clayton, *Corros. Sci.*, 35 (1993) 89
22. H.B. Li, Z. H. Jiang, Y. Yang, Y. Cao, Z. R. Zhang, *Int. J. Min. Met. Mater.*, 16 (2009) 517
23. A. Fattah-alhosseini, M. A. Golozar, A. Saatchi, K. Raeissi, *Corros. Sci.*, 52 (2010) 205
24. J. J. Kim, Y. M. Young, *Int. J. Electrochem. Sci.*, 8 (2013) 11847
25. A. M. P. Simões, M. G. S. Ferreira, B. Rondot, M. da Cunha Belo, *J. Electrochem. Soc.*, 137 (1990) 82
26. C. Escrivà-Cerdána, E. Blasco-Tamarit, D. M. García-García, J. García-Antón, R. Akid, J. Walton, *Electrochim. Acta*, 111 (2013) 552
27. C. Escrivà-Cerdán, E. Blasco-Tamarit, D. M. García-García, J. García-Antón, A. Guenbour, *Corros. Sci.*, 56 (2012) 114
28. C. Escrivà-Cerdán, E. Blasco-Tamarit, D. M. García-García, J. García-Antón, A. Guenbour, *Electrochim. Acta*, 80 (2012) 248
29. C. Escrivà-Cerdán, E. Blasco-Tamarit, D. M. García-García, J. García-Antón, A. Ben-Bachir, *Int. J. Electrochem. Sci.*, 7 (2012) 5754
30. M. BenSalah, R. Sabot, E. Triki, L. Dhouibi, Ph Refait, M. Jeannin, *Corros. Sci.*, 86 (2014) 61
31. M. Boudalia, A. Guenbour, A. Bellaouchou, R. M. Fernandez-Domene, J. Garcia-Anton, *Int. J. Corros.*, 2013 (2013) 1
32. ASTM G-5, Test method for making potentiostatic and potentiodynamic anodic polarization measurements, ASTM, 2004
33. E. A. Abd El Meguid, A. A. Adb El Latif, *Corros. Sci.*, 49 (2007) 263
34. A. Igual Munoz, J. Garcia Anton, J. L. Guinon, V. Perez Herranz, *Corros. Sci.*, 48 (2006) 3349
35. A. Al-Odwani, J. Carew, M. Al-Tabtabaei, A. Al-Hijji, *Desalination*, 135 (2001) 99
36. E. Blasco-Tamarit, A. Igual-Muñoz, J. García Antó, D. Garcia-Garcia, *Corros. Sci.*, 50 (2008) 1848
37. G. C. Palit, V. Kain, H. S. Gadiyar, *Corrosion*, 49 (1993) 977
38. M. V. Cardoso, S. T. Amaral, E. M. A. Martini, *Corros. Sci.*, 50 (2008) 2429

39. D. H. Hur, Y. S. Park, *Corrosion*, 62 (2006) 745
40. J. H. Wang, C. C. Su, Z. Szklarska-Smialowska, *Corrosion*, 40 (1988) 732
41. P. E. Manning, D. J. Duquette, *Corros. Sci.*, 20 (1980) 597
42. G. S. Eklund, *J. Electrochem. Soc.*, 121 (1974) 467
43. G. Wranglen, *Corros. Sci.*, 14 (1974) 331
44. M. Lakatos-Varsányi, F. Falkenberg, I. Olefjord, *Electrochim. Acta*, 43 (1998) 187
45. R. M. Fernandez-Domene, E. Blasco-Tamarit, D. M. Garcia-Garcia, J. Garcia-Anton, *Corros. Sci.*, 52 (2010) 3453
46. J. Kim, S. Pyun, *Electrochim. Acta*, 40 (1995) 1863
47. J. J. Park, S. I. Pyun, W. J. Lee, H. P. Kim, *Corrosion*, 55 (1999) 380
48. T. X. Qiao, Y. G. Zheng, W. Ke, P. C. Okafor, *Corros. Sci.*, 51 (2009) 979
49. G. O. Ilevbare, G. T. Burstein, *Corros. Sci.*, 43 (2001) 485
50. A. Pardoa, M. C. Merino, A. E. Coy, F. Viejo, R. Arrabal, E. Matykina, *Corros. Sci.*, 50 (2008) 1796
51. G. Wranglen, *Corros. Sci.*, 14 (1974) 331
52. Z. Szklarska-Smialowska, *Corrosion*, 28 (1972) 388
53. R. Ke, R. Alkire, *J. Electrochem. Soc.*, 142 (1995) 4056
54. A. Rossi, B. Elsener, G. Hähner, M. Textor, N. D. Spencer, *Surf. Interface Anal.*, 29 (2000) 460
55. J. S. Noh, N. J. Laycock, W. Gao, D. B. Wells, *Corros. Sci.*, 42 (2000) 2069
56. Y. Fu, X. Q. Wu, E. H. Han, W. Ke, K. Yang, Z. H. Jiang, *Electrochim. Acta*, 54 (2009) 1618
57. A. Carnot, I. Frateur, S. Zanna, B. Tribollet, I. Dubois-Brugger, P. Marcus, *Corros. Sci.*, 45 (2003) 2513
58. F. B. Growcock, J. H. Jasinski, *J. Electrochem. Soc.*, 136 (1989) 2310
59. R. Vedalakshm, V. Saraswathy, H. W. Song, N. Palaniswamy, *Corros. Sci.*, 51 (2009) 1299
60. M. Itagaki, A. Matsuzaki, K. Watanabe, *Corros. Sci.*, 37 (1995) 1867
61. E. Almeida, D. Pereira, M. O. Figueiredo, V. M. M. Lobo, M. Morcillo, *Corros. Sci.*, 39 (1997) 1561
62. S. R. Moraes, D. Huerta-Vilca, A. J. Motheo, *Prog. Org. Coat.*, 48 (2003) 28
63. R. A. Antunes, M. C. L. De Oliveira, I. Costa, *Mater. Corros.*, 63 (2012) 586
64. X. Q. Wu, E. H. Han, W. Ke, K. Yang, Z. H. Jiang, *J. Electrochem. Soc.*, 155 (2008) 455
65. A. D. Paola, *Electrochim. Acta*, 34 (1989) 203
66. R. S. Dutt, Jagannath, G. K. Dey, P. K. De, *Corros. Sci.*, 48 (2006) 2711
67. D. D. Macdonald, A. Sun, N. Priyantha, P. Jayaweera, *J. Electroanal. Chem.*, 572 (2004) 421
68. N. B. Hakiki, S. Boudin, B. Rondot, M. Da Cunha Belo, *Corros. Sci.*, 37 (1995) 1809
69. D. D. MacDonald, *J. Electrochem. Soc.*, 139 (1992) 3434
70. D. D. Macdonald, M. U. Macdonald, *J. Electrochem. Soc.*, 137 (1990) 2395
71. J. B. Lee, S. W. Kim, *Mater. Chem. Phys.*, 104 (2007) 98
72. H. B. Li, Z. H. Jiang, H. Feng, H. C. Zhu, B. H. Sun, Z. Li, *Int. J. Min. Met. Mater.*, 20 (2013) 850